Applicability of Benchtop Multi-Wavelength Polar Photometers to Off-line Measurements of the Multi-Angle Absorption Photometer (MAAP) Samples

Sara Valentini[a], Vera Bernardoni[a], Ezio Bolzacchini[c], Davide Ciniglia[a], Luca Ferrero[c], Alice Corina Forello[a], Dario Massabó[b], Marco Pandolfi[d], Paolo Prati[b], Francesca Soldan[a,1], Gianluigi Valli[a], Jesús Yus-Díez[d,e], Andrés Alastuey[d], Roberta Vecchi[a,*]

[a]Department of Physics, Università degli Studi di Milano, and INFN-Milan, via Celoria 16, 20133 Milan, Italy

[b]Department of Physics, University of Genoa and INFN-Genoa, 16146 Genoa, Italy

[c]GEMMA and POLARIS Centre, Università degli Studi di Milano-Bicocca, 20126 Milan, Italy

[d]Institute of Environmental Assessment and Water Research – Spanish National Research Council (IDAEA-CSIC), C. Jordi Girona 18-26, 08034 Barcelona, Spain

[e]Departament of Applied Physics - Meteorology, University of Barcelona, C. Martí i Franquès, 1., 08028, Barcelona, Spain

[1]Present address: Ricerca sul Sistema Energetico - RSE S.p.A., via Rubattino 54, 20134 Milan, Italy

*corresponding author: Roberta Vecchi; roberta.vecchi@unimi.it

Abstract

In this study, the applicability of a benchtop polar photometer (PP_UniMI) to retrieve multi-wavelength aerosol absorption coefficient data by off-line measurements of the Multi-Angle Absorption Photometer (MAAP) sample spots is presented. MAAP is a widespread single wavelength online instrument providing the aerosol absorption coefficient and the equivalent black carbon concentration. In this work, MAAP samples collected during four different campaigns were analysed off-line with PP_UniMI.

First of all, data from PP_UniMI and MAAP were compared to investigate contributions to measurement uncertainties. In particular, the role of the following assumptions performed in the MAAP was investigated:

- reconstructing angular distribution of light scattered by filter samples from measurements at three fixed angles using analytical functions;
- setting the fraction of the back-scattered radiation by the blank filter (B_M) at a fixed value B_M=0.7:
- assuming a fixed value for the asymmetry factor g=0.75.

Samples collected at several sites showed an agreement within 5% when data from the two instruments were retrieved using the same approximations (i.e. backscattered radiation from the filter matrix B_M set at a fixed value, phase functions reconstructed by analytical functions from measurements at 3 angles, same asymmetry factor) in the data retrieval algorithm. Conversely, larger differences (14% on average) between off-line measurements and averaged MAAP data were obtained when the high-angular resolved information available by PP_UniMI was exploited. By analysing the role of MAAP assumptions for σ_{ap} retrieval, it resulted that fixing B_M=0.7 was the main responsible for the detected differences. Indeed, high-angular resolved off-line measurements by PP_UniMI allow to directly measure B_M, obtaining B_M=0.88 on

white spots. It is noteworthy that the observed results were similar at all considered sites, so they proved to be independent of the aerosol type and can likely be attributed to instrumental effects. Moreover, a sensitivity test was carried out also to check the impact of the fixed value used for the asymmetry factor (set at g=0.75 in both instruments). Varying g values within the typical range for ambient aerosol (0.50-0.75) the estimate of aerosol absorbance ABS (directly obtained from PP_UniMI measurements and linked to σ_{ap}) was affected by 8% at most, thus being a minor source of uncertainty in the calculation. The effect of the variability in blank spots used for off-line analyses was also evaluated and resulted in a contribution smaller than 3% to the uncertainty of the methodology employed.

Finally, the possibility of exploiting multi-wavelength assessment of absorption coefficients is an added value of PP_UniMI; indeed, it allows to estimate the contribution of different aerosol sources and components to the absorption coefficient using MAAP tapes used in present or past campaigns.

Keywords

Aerosol absorption coefficient, equivalent black carbon, MAAP, polar photometer, multi-wavelength.

1. Introduction

The study of atmospheric aerosol optical properties (scattering, absorption, extinction) is important to assess the contribution of aerosol-radiation interactions to the Earth radiation balance (IPCC, 2013). Aerosol optical properties depend on the aerosol refractive index, size distribution, and mixing state. Absorbing particles are of particular interest since they have the potential to provide positive contribution to the Earth radiation balance (see e.g. Ferrero et al., 2018). The main absorbing species among aerosol components is black carbon (BC), which is currently identified as the third most important individual climate-warming component (IPCC, 2013). Nevertheless, estimates of the radiative forcing related to BC-radiation interaction are still affected by uncertainties comparable to the estimated value itself (IPCC, 2013) due to the lack of an unambiguous BC definition and difficulties in BC quantification (Petzold et al., 2013), including the evaluation of particle mixing effects on BC absorption properties (Bond et al., 2013; Lack & Cappa, 2010; Samset et al., 2018) and the current absence of a gold-standard reference absorbing material (Baumgardner et al., 2012).

Measurements of the aerosol light absorption coefficient (σ_{ap}) are often carried out using filter-based on-line instruments. Indeed, they allow a relatively easy and unattended operation that makes them suitable for long-term monitoring (Baumgardner et al., 2012). Most on-line filter-based instruments, such as the Aethalometer (Drinovec et al., 2015; Hansen et al., 1984) or the Particle Soot Absorption Photometer – PSAP (Bond et al., 1999), are based on continuous measurements of light transmitted through a filter during sampling and operate at multiple wavelengths. Measurements carried out by these instruments are affected by two artefacts (Weingartner et al., 2003): 1) cross-sensitivities to particle-related scattering and multiple scattering between the aerosol and the substrate; 2) loading effect. Thus, the output of this type of instrumentation must be properly corrected (Collaud Coen et al., 2010; Drinovec et al., 2015; Ogren, 2010; Virkkula et al., 2005). More refined on-line filter-based measurements of σ_{ap} can be obtained by the Multi-Angle Absorption Photometer – MAAP (Petzold & Schönlinner, 2004). This is a single-wavelength instrument that measures both transmitted and scattered light and uses a suitable radiative transfer model to account for multiple scattering effects in order to retrieve the σ_{ap}. The output of the MAAP is the equivalent Black Carbon (eBC) concentration (Petzold & Schönlinner, 2004; Petzold et al., 2013), obtained by σ_{ap} applying a fixed Mass Absorption Cross-section (MAC) of 6.6 m^2/g. As the system accounts for multiple scattering effects and limited loading effect was detected (Petzold et al., 2005), the MAAP has often been considered as reference methodology among on-line filter-based devices providing eBC concentration (Ammerlaan et al., 2017; Müller et al., 2011). Despite MAAP advantages, it is worthy to note that MAAP operates at a single wavelength thus preventing the assessment of aerosol properties and sources linked to wavelength dependence. In addition, previous works evidenced biases affecting eBC values especially at high BC accumulation rate (Hyvärinen et al., 2013); moreover, as in any other filter-based system, the use of a fibre filter might promote sampling artefacts due to the absorption of organics that can affect the estimate of the correct σ_{ap} (Vecchi et al., 2014). Besides on-line measurements, also benchtop laboratory instrumentation has been developed for σ_{ap} measurements on aerosol collected on filters during sampling campaigns. As examples, in-house made polar photometers like the Multi-Wavelength Absorption Analyzer (MWAA) at the University of Genoa (Massabò et al., 2013) and the multi-wavelength polar photometer PP_UniMI at the University of Milan (Bernardoni et al., 2017; Vecchi et al., 2014) have been developed. These instruments allow to determine σ_{ap} at different wavelengths in the range UV-IR based on measurement principles similar to the one of MAAP although implemented differently in each of them; they can analyse filters of different type (e.g. fibre filters/membranes of various size) and also spots (i.e. aerosol deposits) punched from filter tapes.

In this work, the applicability of polar photometers to retrieve multi-wavelength σ_{ap} data from off-line analyses of MAAP spots was investigated. This application is very useful to gain a-posteriori information about the spectral dependence of aerosol light absorption coefficient measured on-line by the single-wavelength MAAP. Indeed, MAAP has been used by many monitoring networks and deployed in a variety of measurement campaigns to obtain eBC or σ_{ap}. The possibility to extend MAAP information at other wavelengths would allow to exploit optical source or component apportionment models such as the Aethalometer model (Sandradewi et al., 2008) or the MWAA model (Massabò et al., 2015); in addition, multi-λ σ_{ap} could be provided and used to test existing correction schemes or retrieve suitable correction factors to be applied to other on-line instruments such as the Aethalometer. It is also noteworthy that

retrospective studies based on measurements performed on MAAP filter tapes collected in past years are also possible. An application of MWAA to obtain multi-wavelength σ_{ap} from MAAP spots is reported by Saturno et al. (2017), who used MWAA measures as multi-λ reference to test two different Aethalometer correction schemes in terms of the Absorption Ångström Exponent (AAE).
To test the robustness of this methodology and application, different contributions to measurement uncertainties were investigated. Data collected during four sampling campaigns deploying the MAAP were analysed and off-line data measured by PP_UniMI were compared to average values obtained by the MAAP for each spot. Results of this inter-comparison, a study of the effect of assumptions in the MAAP retrieval algorithm, and sensitivity tests to the radiative transfer model input data and parameters are also presented. Although it is more time-consuming than on-line absorption photometers, the off-line multi-wavelength analysis of MAAP spots by PP_UniMI provides more robust results as it relies on fewer assumptions; in addition, it does not need a-posteriori empirical corrections for multiple scattering effect, which is a critical artefact in photometers based on transmission only as already outlined by many studies (e.g. Bond et al., 1999; Collaud Coen et al., 2010; Ogren, 2010; Saturno et al., 2017; Virkkula et al., 2005; Weingartner et al., 2003).

2. Material and Methods

In the following, details about instruments, off-line measurements, sampling sites, and aerosol types are given.

2.1 The Multi-Angle Absorption Photometer (MAAP)

The Multi Angle Absorption Photometer (MAAP, Thermo Scientific) is an on-line instrument based on simultaneous measurements of light transmitted and scattered by the aerosol continuously collected on a glass-fibre filter tape to determine eBC content. In order to avoid issues related to loading effects, the filter tape is moved whenever light transmittance through the filter is reduced to a fixed percentage of the initial value (default: 20%). After the measurement, the filter tape with aerosol deposits (hereafter called "spots") can be removed from the sampler and spots can be punched from the tape. Few literature studies (e.g. Nordmann et al., 2009; Saturno et al., 2017) report off-line analyses carried out on MAAP spots, but these measurements are scarce and not routinely performed.
The MAAP (λ = 637 ± 1 nm, Müller et al., 2011) measures light transmitted and scattered at three angles (0°, 130°, and 165°) properly selected. These measurements allow the reconstruction of the total light diffused in the forward and backward hemispheres integrating suitable analytical functions (Petzold & Schönlinner, 2004). Such measurements are performed on blank (i.e. before sampling) and loaded (i.e. while sampling) filters; these data are the input to the radiative transfer model reported by Hänel (1987,

1994) for membrane filters and extended by Petzold & Schönlinner (2004) to fibre filters. In the algorithm, fixed values for the fraction of the radiation back-scattered by filter matrix (B_M) and the asymmetry factor (g) are imposed a-priori. The radiative transfer model provides the aerosol absorbance (ABS) of the sample. The deposit area and sampling air flow are used to retrieve σ_{ap} from ABS. The output of the instrument is the atmospheric eBC concentration (in µg/m^3), which is obtained from σ_{ap} setting a value for the black carbon Mass Absorption Cross-section (MAC=6.6 m^2/g is set by the manufacturer) (Petzold et al., 2002). Petzold & Schönlinner (2004) reported that sensitivity tests on all these assumptions resulted in an overall uncertainty of 12% in the MAAP output. In particular, the hypotheses on the angular distribution of scattered light and the asymmetry factor g produced an uncertainty of 5% each, while the uncertainty associated to the fixed B_M value was estimated to be 10%. Moreover, a sensitivity test on B_M showed that a 1% uncertainty on B_M resulted in an approximately 1% uncertainty on ABS value. Further details on the performance of the instrument can be found in Müller et al. (2011).

As already mentioned, in the MAAP the filter tape is moved whenever the transmittance measurement is reduced to a fixed value to limit problems related to filter loading. Nevertheless, Hyvärinen et al. (2013) pointed to possible issues with measurements - especially at high σ_{ap} – likely related to erroneous dark counts in the photodetector measuring the transmitted light, and an internal averaging procedure of the photodetector raw signals. The authors developed a correction algorithm to get rid of them. In this work, no correction was applied to MAAP outputs; however, to avoid biases caused by high BC concentrations, all data resulting in $\sigma_{ap} > 60$ Mm^{-1} were neglected. Indeed, a lack of linearity in the MAAP response was observed above this threshold: when compared to off-line measurements, MAAP apparently underestimated higher σ_{ap} values. Note that, considering the flow rates used for MAAPs employed in the present study (in the range 0.9-1 m^3/h), this is in agreement with the limit reported by Hyvärinen et al. (2013) above which MAAP is expected to underestimate BC concentrations, corresponding to 55-62 Mm^{-1} depending on the flow rate.

The data presented in this paper are referred to samples collected by three MAAPs, operating at sites with different characteristics in various campaigns (see Section2.3). At the end of the campaigns, the filter tapes were removed from the MAAP and spots were punched to 22 mm diameter (fully including the aerosol spot) for the off-line analysis by PP_UniMI and compared to MAAP results (see Section 2.2). To allow the comparison with off-line measurements, the average σ_{ap} for each MAAP spot (hereafter called σ_{ap_MAAP}) was calculated as $\sigma_{ap\_MAAP}=\langle eBC\rangle_t\cdot MAC$, where $\langle eBC\rangle_t$ is the on-line eBC concentration given by the MAAP averaged over each spot sampling time (t) and the MAC value was the one set by the manufacturer.

2.2 The polar photometer PP_UniMI

PP_UniMI is a multi-wavelength polar photometer developed at the University of Milan. Details on the instrument can be found in Bernardoni et al. (2017) and Vecchi et al. (2014), thus only a brief summary of measurement principles will be given here.

Similarly to the MAAP, PP_UniMI is based on the detection of the amount of light scattered in the forward and backward hemispheres by blank and loaded filters to assess σ_{ap} of aerosol collected on filters. The instrument currently operates at 405 nm, 448 nm, 532 nm, 635 nm, and 780 nm; measurements at 635 nm only will be presented in this work, for sake of comparison with the MAAP (operating at 637 nm – see Section2.1). Note that no wavelength correction was applied to avoid further assumptions; anyway, the 2 nm λ discrepancy between MAAP and PP_UniMI would lead to a difference smaller than 1%. The main difference with the MAAP approach is that high angular resolution measurements are performed by PP_UniMI. Indeed, PP_UniMI measures the light intensity on the scattering plane from 0° to 173° with about 0.4° resolution, by an amplified photodetector mounted on a rotating arm. The same analytical function (i.e. a linear combination of a cosine and a Gaussian) used in the MAAP to represent the angular distribution of back-scattered light is employed to reconstruct the signal from 173° to 180°; sensitivity tests on the effect of the function (cosine-Gaussian combination or parabola) chosen for the 173-180° signal reconstruction resulted in a σ_{ap} variability within 0.1% at all wavelengths. The sample under analysis coincides with the rotation centre. The amount of light scattered in the forward and backward hemispheres is then obtained by solid-angle integration. QA/QC procedures ensure the quality of measurements, i.e. laser intensity is monitored before and after each measurement session and it is used to normalise measurements to a reference value.

The total amount of light scattered in the two hemispheres by blank and loaded spots is measured and used as input to the same two-layer radiative transfer model as the one implemented in the MAAP (Hänel, 1987, 1994; Petzold & Schönlinner, 2004) obtaining ABS for each analysed sample. Estimates for limits of detection and uncertainties on ABS can be found in Bernardoni et al. (2017).

As already mentioned, polar photometers can be exploited to perform measurements of standard filters and sample spots produced by commercially available on-line instrumentation, such as MAAP, to gain additional information and insights into e.g. filter-based photometers correction schemes (Saturno et al., 2017; Bernardoni et al., 2020). In this work, sample spots punched from the MAAP filter tape were analysed with PP_UniMI. Furthermore, also blank parts of the filter tape (located just before or immediately after the part of the tape containing the spots to be analysed) were punched, analysed, and averaged to obtain a representative blank necessary to run the radiative transfer model.

Once ABS for each spot was retrieved, to calculate σ_{ap} for each spot measured by PP_UniMI (hereafter called $\sigma_{ap\_PP\_UniMI}$), the sampling volume was obtained as V=F·t, where F is the MAAP flow rate and t is the time-lapse of the sampling for each spot. MAAP spot area (A) was determined by repeated measurements of spot diameters and ranged from 2.02 to 2.09 cm^2 (depending on the MAAP instrument used in the campaigns); instrument-specific A and F values were used in data analysis. Finally, $\sigma_{ap\_PP\_UniMI}$ was calculated as $\sigma_{ap\_PP\_UniMI}$=ABS·A/V.

In this work, aiming at an application of polar photometry to provide additional information from MAAP spots, all contributions to measurement uncertainties were evaluated. In particular, the effect of assumptions made by the MAAP to measure σ_{ap} was specifically investigated. Indeed, while PP_UniMI basically measures the full angular distribution of radiation scattered from the filter, MAAP retrieves the angular distribution of scattered light making use of analytical functions and measurements at three fixed angles (see Sections 2.1 and 2.2). To analyse PP_UniMI measurements on MAAP spots using the same assumptions as the MAAP, it is possible to consider values of the signal measured by PP_UniMI photodiode at the same scattering angles as those set in the MAAP and reconstruct the angular distribution of scattered light with the same functions; in addition, when applying the radiative transfer algorithm, values of B_M and g can be set equal to the ones fixed in the MAAP (0.7 and 0.75, respectively – Petzold et al., 2002; Petzold & Schönlinner, 2004). This data analysis approach will be called "PP_UniMI as MAAP" (PaM) in the following; the aerosol absorption coefficient calculated with this method will be referred to as σ_{ap_PaM}.

To further investigate the impact of the different MAAP hypotheses separately, two additional tests were performed:

1. angular distributions of scattered light were reconstructed as performed by the MAAP but, instead of using a fixed B_M, it was experimentally determined by the integrals of these distributions (calculated following Petzold & Schönlinner, 2004); the nomenclature for the aerosol absorption coefficient will be $\sigma_{ap\_PP\_fun}$ in this case. Indeed, with this data analysis approach (hereafter called PP_fun), PP_UniMI data were employed to highlight the effect of using analytical functions to reconstruct the scattered light angular distribution (see Section 3.2.1);
2. full angular distributions directly measured by PP_UniMI were employed and B_M was set equal to 0.7 (as in the MAAP); the symbol $\sigma_{ap\_PP\_BMfix}$ will be used. This approach (called PP_BMfix in the following) was employed to single out the impact of the fixed B_M value in the MAAP algorithm (see Section 3.2.2).

A summary of inputs used in each of the tests described above is reported in Table 1.

Note that this investigation of the effect of the MAAP hypotheses on the angular distributions of light scattered by blank and loaded spots was performed considering the same value for the asymmetry factor as the one set in the MAAP in all calculations. In order to single out the sensitivity of MAAP radiative transfer algorithm also to this assumption, tests were carried out to retrieve σ_{ap} using different g values in a range found in the literature for ambient aerosol (see Section3.2.3). In this case, both PaM and PP_UniMI approaches were employed in the analysis.

Finally, as MAAP blank spots corresponding to each loaded one are no more available after sampling (see Section 2.1) and other parts of the tape have to be used as representative blank filters (see Section 2.2), the variability among different blank spots was evaluated and its effect was investigated using PaM and PP_UniMI approaches.

Table 1 Nomenclature used throughout the paper for the calculation approaches tested to retrieve σ_{ap} from PP_UniMI measurements of MAAP spots.

Approach nomenclature	B_M	Angular distributions of scattered light
PP_UniMI	Experimental	Experimental, high angular resolution
PaM	Fixed (0.7)	Reconstructed from data at 3 angles
PP_fun	Experimental	Reconstructed from data at 3 angles
PP_BMfix	Fixed (0.7)	Experimental, high angular resolution

2.3 Sampling sites and campaigns

Figure 1 Location of sampling sites where MAAP samples were collected.

2.3.1 Urban background sites in Milan (Italy)

A sampling campaign was performed in 2016 on a balcony (about 3 m a.g.l.) at the Department of Physics of the University of Milan (hereafter called “UniMI” site). This can be considered an urban background site since it is located far from direct emission sources such as vehicular traffic. The PM_{10} campaign at UniMI was carried out from November 21st to December 23rd. Eighty-six MAAP spots among all those collected during this campaign were analysed by PP_UniMI.

Another sampling campaign was performed on the rooftop (10 m a.g.l.) of the U9 building at the University of Milano-Bicocca, an urban background station located inside the university campus (it will be referred to as "UniBIC" in the following). $PM_{2.5}$ measurements were performed in the frame of the EMEP/ACTRIS/COLOSSAL winter campaign in Milan (Bernardoni et al., 2019; Bernardoni et al., 2020; Ferrero et al., 2019; Ferrero et al., in preparation) from January 17th to 31st 2018. Thirty-eight MAAP spots among all those collected during this campaign were analysed.

During UniMI and UniBIC campaigns, a MAAP mod. 5012 (λ=637±1 nm) operating with a flow rate F=1 m^3/h was employed.

2.3.2 Urban background site in Barcelona (Spain)

The Environmental Geochemistry and Atmospheric Research (EGAR) Group of the Institute of Environmental Assessment and Water Research (IDAEA-CSIC) measures multiple aerosol properties at an urban background site located within the grounds of the IDAEA research centre in Barcelona - Spain (hereafter "BCN"). This site is part of the Catalonian Air Quality Monitoring Network. The filter spots collected ranged from October 22nd 2018 to June 11th 2019. Eighty-five MAAP spots among all those collected during the campaign were analysed by PP_UniMI.

A MAAP mod. 5012 (λ=637±1 nm) was employed to sample PM_{10} with a flow rate of 1 m^3/h during the BCN campaign.

2.3.3 Regional background site in Montseny (Spain)

Measurements from June 19th to December 29th 2018 were performed at Montseny ("MSY" in the following) regional background supersite located in a valley in the Pre-Coastal Catalan mountain range, 50 km to the N–NE of the Barcelona, and 25 km from the Mediterranean coast. This supersite is part of the Catalonian Air Quality Monitoring Network and are part of ACTRIS and GAW networks. Among all the MAAP filter tape spots collected, 123 were analysed by PP_UniMI.

At MSY, a MAAP mod. 5012 (λ=637±1 nm) operating with a flow rate F=0.9 m^3/h was employed downstream a drier during a PM_{10} campaign.

3. Results and Discussion

3.1 Comparison between spot measurements by PP_UniMI and MAAP outputs

Data from all sampling campaigns considered in this study were aggregated; $\sigma_{ap\_PP\_UniMI}$ and σ_{ap_MAAP} obtained as explained in Section 2.2 were compared as shown in Figure 2. As both PP_UniMI and MAAP data are affected by non-negligible uncertainties, a Deming regression was performed with the R (R Core Team, 2020) package "deming" (Linnet, 1990; Ripley & Thompson, 1987) considering measurement uncertainties on x and y variables, i.e. 12% on both $\sigma_{ap\_PP\_UniMI}$ and σ_{ap_MAAP} in addition to 1 Mm^{-1} to take into account larger uncertainties at low σ_{ap} values. Please note that the same approach was considered in all regression analyses when comparing σ_{ap} measured with PP_UniMI on MAAP spots and averaged MAAP output (σ_{ap_MAAP}).

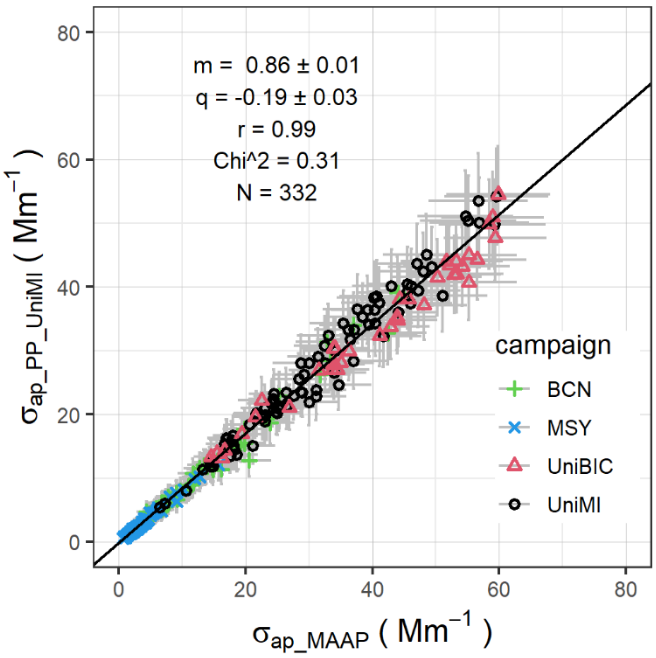

Figure 2 Comparison between the aerosol absorption coefficient measured by PP_UniMI on sample spots ($\sigma_{ap\_PP\_UniMI}$) and the one obtained from MAAP output (σ_{ap_MAAP}). Data from all sampling campaigns presented in this study are represented with different point shapes and colours. m and q are the slope and intercept of the regression (± 1 standard error), respectively; r is the correlation coefficient between x and y variables; Chi^2 is the value of the reduced Chi squared; N is the number of data points.

The difference between MAAP outputs and PP_UniMI measurements on MAAP spots was 14% considering the regression slope: this discrepancy slightly exceeded the estimated MAAP overall uncertainty (12% - Petzold & Schönlinner, 2004), hence it will be investigated further in the next sections. It is noteworthy that the observed MAAP overestimation was similar if data of the different sampling campaigns and sites were considered separately, being in the range 13-21%. Indeed, analogous regression analyses performed for each of the four datasets showed slightly different slopes: 0.87 (UniMI), 0.83 (UniBIC), 0.82 (BCN), and 0.79 (MSY) and intercepts comparable to zero within three standard errors. In all cases, the correlation was excellent (correlation coefficient r>0.98).

These results showed that there was neither evidence of effects related to the aerosol type sampled by the MAAP nor influence of the filter tape in use.

Overestimations of σ_{ap_MAAP} compared to σ_{ap} measured by other instruments or techniques were already reported in some literature studies and inter-comparison experiments. For instance, Park et al. (2006) showed that for ambient aerosol sampled at the Fresno Supersite (U.S.) linear regression analyses between σ_{ap} measured by the MAAP (y) and a photoacoustic analyser (x) had slopes 1.23 and 1.52 (and positive intercepts) during summer and winter campaigns, respectively. Also Chow et al. (2009) reported an average 51% MAAP overestimation compared to photoacoustic at the same site. More recently, other studied have evidenced values of σ_{ap_MAAP} higher than σ_{ap} obtained for ambient aerosol by a CAPS PMssa Monitor (15% overestimation - Modini et al., 2018) and off-line analyses performed with the in-house made photometer MWAA on filter samples collected in parallel (slope of regression MAAP vs MWAA 1.16 and positive intercept - Saturno et al., 2017). More variable results were found for laboratory aerosols. Sheridan et al. (2005) discovered a slight overestimation of σ_{ap_MAAP} compared to a reference in-situ absorption measurement ($\sigma_{ap\_MAAP}=1.04\cdot\sigma_{ap\_reference}+1.00$), whereas Slowik et al. (2007) showed that MAAP values were 20% higher and 7% lower than those given by a photoacoustic spectrometer for kerosene soot and glassy carbon spheres, respectively. Weber et al. (2019) highlighted differences in MAAP response compared to Extinction-minus-Scattering method from -5% (for flame soot) to +20% (for Carbon Black particles). Note that, especially when ambient aerosol is sampled, a concurrent cause of MAAP overestimation compared to in-situ data may be the effect of sampling artefacts, that can increase the σ_{ap} measured on a fibrous matrix with respect to the one determined on membrane filters (Vecchi et al., 2014) or by in-situ techniques.

3.2 Insights into MAAP retrieval algorithm

To investigate the whole effect of assumptions on the angular distributions and the B_M value implemented in the MAAP algorithm, spots measured by PP_UniMI were analysed using the PaM approach. The comparison between aerosol absorption coefficient inferred from this method (σ_{ap_PaM}) and MAAP outputs (σ_{ap_MAAP}) is represented in Figure 3. A Deming regression was performed considering measurement uncertainties on both variables (see Section 3.1).

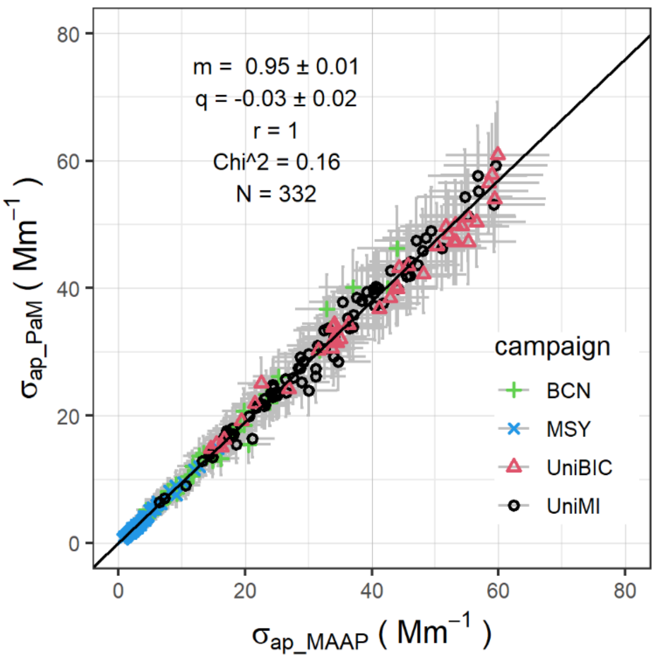

Figure 3 Comparison between the aerosol absorption coefficient measured by PP_UniMI on sample spots analysed using reconstructed angular distributions and B_M=0.7 (σ_{ap_PaM}) and the one obtained from MAAP output (σ_{ap_MAAP}). Data from all sampling campaigns presented in this study are represented with different point shapes and colours. m and q are the slope and intercept of the regression (± 1 standard error), respectively; r is the correlation coefficient between x and y variables; Chi^2 is the value of the reduced Chi squared; N is the number of data points.

It can be noted that when using the PaM approach, the difference between MAAP outputs and results of PP_UniMI analyses on MAAP spots reduced from 14% to 5%, which is largely within instrumental uncertainties, and the intercepts observed were all comparable to zero within three standard errors. Considering data from different campaigns separately, slopes of regression analyses were in the range 0.94-0.96, hence discrepancies in the range 4-6% were found between PaM and MAAP, showing that the effect of MAAP assumptions was independent of the site, the aerosol type, and the specific filter tape in use. Additional analyses and sensitivity tests were performed to figure out the effect on the instrument output in relation to the two main hypotheses in the MAAP algorithm (fixed B_M and angular distribution reconstruction) separately as described in Section 2.2. Results are reported in the next paragraphs.

3.2.1 Effect of reconstructing the angular distribution of scattered light

Figure 4 shows an example of the angular distribution of the radiation scattered by a MAAP sample spot as measured by PP_UniMI with high angular resolution (dotted line) and reconstructed using signals measured at 0°, 130° and 165° and the analytical functions employed by the MAAP (solid line, PaM approach). Data were separately normalised to the maximum values in the two hemispheres for sake of clarity of the Figure.

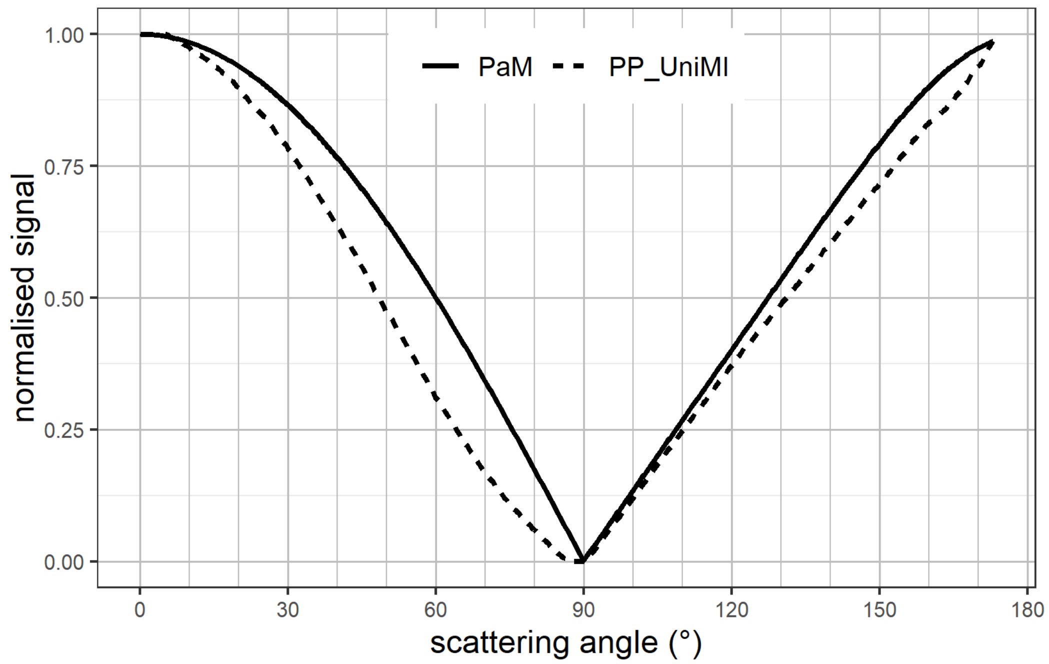

Figure 4 Angular distribution of light scattered by a MAAP spot measured by PP_UniMI and reconstructed using MAAP analytical functions from signals at 3 angles (PaM – solid line) and as directly measured by PP_UniMI with high angular resolution (PP_UniMI – dotted line).

It is noteworthy that measured and reconstructed angular distributions were different, especially in the forward hemisphere, where the perfectly Lambertian diffusion approximation appeared to be incorrect. Discrepancies between the two angular distributions were evaluated in terms of integrals of radiation scattered in the forward (P) and backward (B) hemispheres, i.e. the quantities employed in MAAP radiative transfer algorithm. Note that these integrals were calculated differently in the PaM and PP_UniMI approaches: in the former case, equations (4) and (5) from Petzold & Schönlinner (2004) were applied to the reconstructed data, while in the latter solid-angle integrals of directly measured angular distributions were calculated. To allow a direct comparison between the two integrals, a normalisation procedure was applied. The total amount of light scattered (forward+backward hemispheres) (P+B) was calculated using both PP_UniMI (P+B_PP) and PaM (P+B_PaM) methods; considering PP_UniMI as the reference in this case, the normalisation factor N=(P+B_PaM)/(P+B_PP) was used to scale light scattered in each hemisphere computed with the PaM approach for N, thus allowing to evaluate differences between the mentioned integrals.. All available spots were used for this analysis. For both blank and loaded spots, the largest relative difference was observed in the forward hemisphere where the scattered radiation calculated from reconstructed angular distributions was on average 18% and 17% higher than the one obtained exploiting PP_UniMI high angular resolution for blank and sampled spots, respectively (with a slightly different 95% confidence interval CI: 13-26% and 13-21% for blank and loaded spots, respectively). Conversely, the analogous difference in the backward hemisphere was -2% for both blank and loaded spots, with a variability smaller than 1%. Finally, it has to be noted that, even though the observed discrepancy was significant in the forward hemisphere, the MAAP and PP_UniMI radiative transfer scheme takes into account only the ratios of radiation scattered by loaded to blank spots separately for the two hemispheres, i.e. $P_F/P_F^{(0)}$ and $B_F/B_F^{(0)}$ (where superscript "(0)" indicates the blank filter and subscript "F" denotes the whole filter – comprising also the layer with particles if loaded) (Hänel, 1987; Petzold & Schönlinner, 2004). Table 2 reports average values for $P_F/P_F^{(0)}$ and $B_F/B_F^{(0)}$ calculated exploiting full PP_UniMI angular resolution (PP_UniMI) and MAAP angular distributions reconstruction (PaM). These ratios were evaluated considering P_F and B_F for each loaded spot and campaign-averaged $P_F^{(0)}$ and $B_F^{(0)}$ (as no blank spot corresponding to each loaded one was available – see also Section 2.2) Note that the large standard deviations reflect the variability in aerosol loading among all black spots considered in this study.

Table 2 Average (± 1 standard deviation) of $P_F/P_F^{(0)}$ and $B_F/B_F^{(0)}$ calculated for all 332 available spots using the PaM and PP_UniMI approaches.

	PaM	**PP_UniMI**
$P_F/P_F^{(0)}$	0.38±0.13	0.38±0.14
$B_F/B_F^{(0)}$	0.53±0.14	0.52±0.14

Differences between $P_F/P_F^{(0)}$ and $B_F/B_F^{(0)}$ calculated using PP_UniMI and PaM methodologies were found out to be negligible (95% CI: -4% - +5% in the forward hemisphere; -3% - +4% in the backward one). Therefore, it was expected that the observed discrepancy in angular distributions of scattered light had a small effect on σ_{ap_MAAP} retrieved by the MAAP; to investigate this hypothesis, the PP_fun approach was used (i.e. distribution of scattered light reconstructed using analytical functions, see Section 2.2). Figure 5 shows the comparison between the $\sigma_{ap\_PP\_fun}$ and σ_{ap_MAAP}.

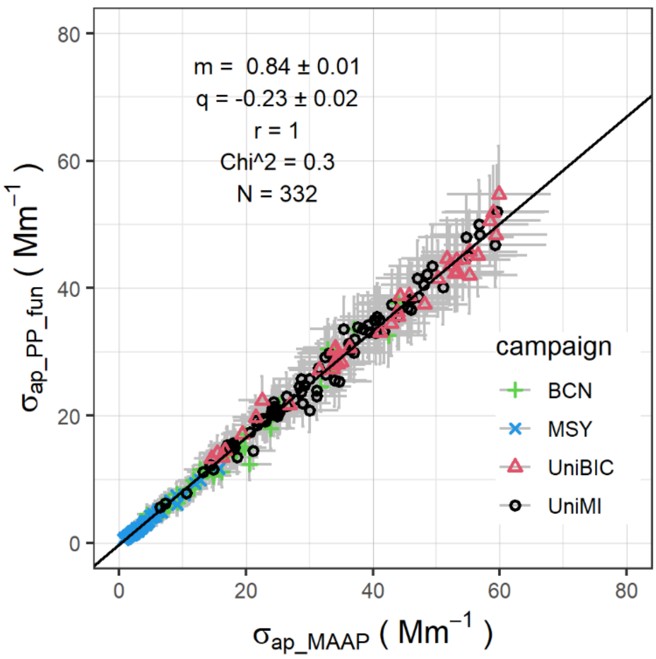

Figure 5 Comparison between the aerosol absorption coefficient obtained using the PP_fun approach ($\sigma_{ap\_PP\_fun}$) and the one obtained from MAAP output (σ_{ap_MAAP}). Data from all sampling campaigns presented in this study are represented with different point shapes and colours. m and q are the slope and intercept of the regression (± 1 standard error), respectively; r is the correlation coefficient between x and y variables; Chi^2 is the value of the reduced Chi squared; N is the number of data points.

The PP_fun approach gave the same response (within 3%) as the standard PP_UniMI methodology compared to MAAP outputs (see also Figure 2). Note that, considering the different sampling campaigns separately, analogous regression analyses showed slopes slightly higher (0.84±0.01) for the urban background sites in Milan and lower for BCN and MSY sites (0.79 and 0.76, respectively) with intercepts comparable to zero.

The only difference between the PP_fun and the PP_UniMI approaches was in the retrieval of the angular distribution of scattered light; even though measured and reconstructed angular distributions were different (see Figure 4), this did not affect the retrieval of aerosol absorption coefficient for more than 5%, which is comparable with the unit-to-unit variability among different MAAP instruments estimated in inter-comparison studies (see e.g. *ACTRIS*, 2013; Müller et al., 2011).

3.2.2 Effect of the fixed B_M value

Taking into account all 51 blank spots available from the sampling campaigns presented in this paper, B_M measured by PP_UniMI for the filter tape in use was on average 0.88±0.01, ranging between 0.86 and 0.89, when full angular resolution was employed; in case the MAAP angular distribution reconstruction was performed, B_M=0.85±0.01 (range 0.84-0.87) was obtained. Thus, the B_M=0.7 fixed in the MAAP did not appear to be adequate for the filter tape currently employed in the MAAP, and this was valid for all instruments and filter tapes available in the various campaigns.

As explained in Section 2.2, the PP_BMfix approach was employed to evaluate the effect of the fixed B_M in the MAAP algorithm. A comparison of aerosol absorption coefficient obtained with the PP_BMfix methodology and the one inferred from MAAP outputs is shown in Figure 6.

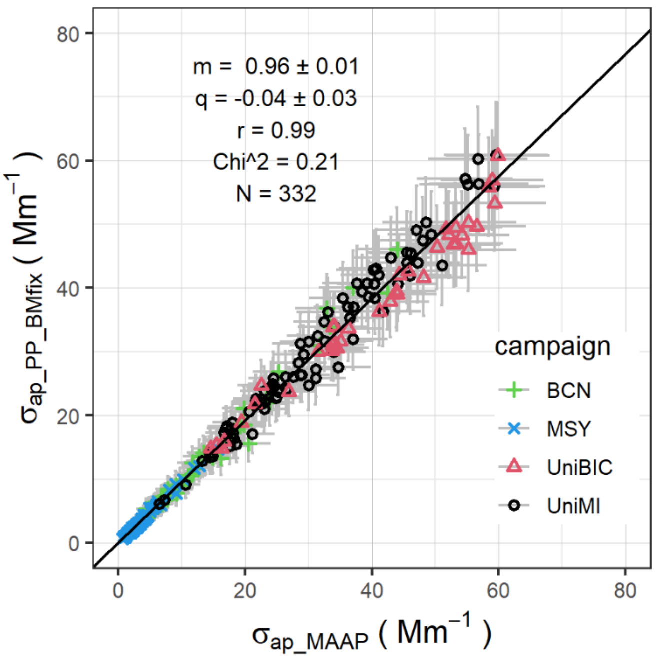

Figure 6 Comparison between the aerosol absorption coefficient obtained using the PP_BMfix approach ($\sigma_{ap\_PP\_BMfix}$) and the one obtained from MAAP output (σ_{ap_MAAP}). Data from all sampling campaigns presented in this study are represented with different point shapes and colours. m and q are the slope and intercept of the regression (± 1 standard error), respectively; r is the correlation coefficient between x and y variables; Chi^2 is the value of the reduced Chi squared; N is the number of data points.

PP_BMfix results were comparable with PaM ones within 1% (see also Figure 3). If the different sampling campaigns were considered separately, analogous regression analyses exhibited similar slopes: 0.97 (UniMI), 0.93 (UniBIC), 0.97 (BCN), and 0.95 (MSY).

This result suggests that, among the assumptions introduced in the MAAP algorithm to calculate σ_{ap}, fixing B_M=0.7 is the hypothesis that contributes at most to the observed discrepancy with results of PP_UniMI analyses. Indeed, when considering only reconstructed angular distributions of scattered light (i.e. the only approach that can be implemented in the MAAP due to the limited angular resolution), it should be observed that the difference between calculating B_M as done in the PP_fun calculation method and fixing B_M=0.7 as done in the PaM approach plays an important role: σ_{ap} values comparable with MAAP outputs (within 5%) were only obtained when the same MAAP assumption on B_M was employed in spots data analysis. To highlight the effect of different B_M settings, a Deming regression was performed between σ_{ap} retrieved with the B_M (0.85 on average) calculated from reconstructed angular distributions ($\sigma_{ap\_PP\_fun}$) and obtained using B_M=0.7 (σ_{ap_PaM}); the regression exhibited a slope of 0.88±0.01 and a small intercept (-0.21±0.01 Mm^{-1}), indicating that the hypothesis on B_M currently used in the MAAP can cause an overestimation of about 12% (ranging between 11% and 19% considering slopes of the same regression for different campaigns separately) of the σ_{ap} (and thus of eBC concentration).

3.2.3 Sensitivity tests on asymmetry factor assumption

As mentioned in Sections 2.1 and 2.2, in the MAAP retrieval algorithm a fixed value of the asymmetry factor is set. Indeed, this parameter is the only quantity that has to be assumed in the radiative transfer scheme implemented in the instrument (Hänel, 1987) and it cannot be obtained as model output. A value of g=0.75 is set in the MAAP as it is considered representative of average ambient urban aerosol, characterised by a range of asymmetry factors from 0.65 to 0.86 as reported by Petzold & Schönlinner (2004) and references therein. A recent study (Moosmüller & Ogren, 2017) summarised that typical values for ambient aerosol asymmetry parameter (at 550 nm wavelength) vary from 0.26 to 0.80 based on a review of previous literature works that made use of multiple approaches to calculate g at several sites. Taking into account values most frequently found in the literature, a range of g from 0.35 to 0.75 was employed in this study to test MAAP sensitivity to different g values. Moreover, the g interval 0.50-0.75 was analysed in detail since this range is in agreement with the variability of asymmetry factor observed across Europe (Pandolfi et al., 2018) and because values of g larger than 0.50 have often been reported in the literature (see e.g. Andrews et al., 2006; D'Almeida et al., 1991; Donateo et al., 2018; Formenti et al., 2000; Hartley & Hobbs, 2001; Horvath et al., 2016; Horvath et al., 2018; Gopal et al., 2014). Data obtained from PP_UniMI measurements of MAAP sample spots were analysed with both PaM and PP_UniMI methods; in this sensitivity test, aerosol absorbance ABS was the quantity of interest because it is the one directly obtained from PP_UniMI measurements and to avoid additional uncertainties related to air flow and spot areas. When comparing ABS calculated using different input g values, the uncertainties used in Deming regressions were 10% plus a fixed 0.01 for both x and y variables.

Absorbances calculated with tested g values (hereafter $ABS_{\_PaM\_gX}$, where X stays for the tested g) were compared to those obtained considering the standard g=0.75 ($ABS_{\_PaM}$). For the PaM approach, Deming regression parameters of the comparison $ABS_{\_PaM\_g0.35}$ (y) vs $ABS_{\_PaM}$ (x) were m=1.145±0.001 (slope) and q=-0.016±0.001 (intercept); for the PP_UniMI method, the Deming regression $ABS_{\_PP\_UniMI\_g0.35}$ (y) vs $ABS_{\_PP\_UniMI}$ (x) parameters were m=1.119±0.001 (slope) and q=-0.015±0.001 (intercept); note that the small intercepts were both lower than PP_UniIMI ABS LOD at 635 nm (0.03 – see Bernardoni et al. (2017)). Moreover, when using g>0.50, Deming regression parameters of $ABS_{\_PaM\_g0.50}$ (y) vs $ABS_{\_PaM}$ (x) were m=1.082±0.001 (slope) and q=-0.010±0.001 (intercept) and those of the comparison $ABS_{\_PP\_UniMI\_g0.50}$ (y) vs $ABS_{\_PP\_UniMI}$ (x) were m=1.064±0.001 (slope) and q=-0.009±0.001 (intercept).

It is noteworthy that, considering both g=0.35 and g=0.50, PP_UniMI approach response to g variations compared to g=0.75 was smaller than the one of PaM approach.

These results highlight that the MAAP algorithm appears less sensitive to the asymmetry factor set in the algorithm than to the fraction of radiation backscattered by the blank filter (B_M – see Section 3.2). Indeed, using a g value at a reasonable lower limit for ambient aerosol (g=0.50), the radiative transfer scheme response varied no more than 8% compared to g=0.75 as set in the instrument (considering the regression slope); furthermore, ABS change was reduced to 6% if PP_UniMI approach was employed together with g=0.50.

3.3 Effect of blank filter variability

As explained in Section 2.2, to retrieve ABS of MAAP samples with PP_UniMi some spots were punched from blank parts of the filter tape; afterwards, they were measured and their scattered light angular distribution was averaged to obtain representative blank filter input quantities to be included in the radiative transfer scheme together with those of loaded spots. However, the on-line absorbance obtained by the MAAP is calculated using as blank filter the one analysed immediately before sampling (i.e. the blank spot soon after filter tape advance). It is therefore clear that, using an average blank spot, PP_UniMI results could be biased by the variability in the angular distribution of light scattered by blank filters due to possible tape inhomogeneities. This point was investigated computing the total (forward+backward hemispheres) solid-angle integrals of light scattered by all 51 blank spots available from the considered campaigns. The average variability in total light scattered by blank spots was less than 5% independently of the use of analytical functions to reconstruct angular distributions or PP_UniMI high-angular resolution data.

A sensitivity test on ABS response to a similar change in blank spots was performed: for each campaign, the total solid-angle integral of light scattered by the average blank spot was decreased and increased by 5% and ABS for each sample spot was re-calculated. These ABS values were then compared to those retrieved using the original average blank filters parameters and Deming regressions considering measurement uncertainties (10% plus 0.01) on x and y variables were performed. Both PaM and PP_UniMI approaches showed similar results: slopes and intercepts of the ABS(blank+5%) vs ABS regressions were (m=1.026±0.001; q=0.016±0.001) and (m=1.029±0.001; q=0.015±0.001) for PaM and PP_UniMI approaches, respectively, while those of the ABS(blank-5%) vs ABS regressions were (m=0.973±0.001; q=-0.016±0.001) (PaM) and (m=0.970±0.001; q=-0.015±0.001) (PP_UniMI). Therefore, blank filter variability is a small contribution to the uncertainty of PP_UniMI measurements of MAAP sample spots, affecting results by less than 3% considering regression slopes.

4. Conclusions

In this study, the applicability of in-house made polar photometers to retrieve off-line multi-λ aerosol absorption coefficient (σ_{ap}) from the Multi-Angle Absorption Photometer (MAAP) aerosol deposits (spots) was investigated. To test the robustness of these measurements, different contributions to σ_{ap} uncertainty were examined. In particular, the role of the approximations introduced in the algorithm implemented in the MAAP to obtain σ_{ap} was investigated. More in detail, the effect of:

- reconstructing the angular distribution of radiation scattered by the sample from measurements of light intensity at 3 fixed angles using analytical functions;
- fixing the fraction of backscattered light from the blank filter as B_M=0.7;
- setting the asymmetry factor g=0.75

was analysed separately.

Finally, the role of using an average blank spot in the analysis (i.e. the only possibility for off-line measurements) was explored.

This investigation was performed by means of measurements of the angular distribution of light scattered by MAAP filter tape spots carried out with high angular resolution by the in-house made polar photometer PP_UniMI. Comparisons of PP_UniMI results with MAAP outputs evidenced that the hypotheses employed in the MAAP retrieval algorithm may play an important role. In particular, the study pointed out that, among the previously mentioned hypotheses, fixing B_M=0.7 affected σ_{ap} obtained from MAAP data most (on average 14%). Indeed, blank spots measured by PP_UniMI showed B_M=0.88 (0.85 if calculated from data at MAAP three angles), which is significantly higher than the value commonly employed in the MAAP (0.7). As already pointed out by Petzold & Schönlinner (2004), a difference in B_M with respect to the fixed B_M=0.7 (the value of 0.85 calculated from MAAP reconstructed angular distributions is 21% higher) causes a bias of a similar magnitude in the aerosol absorbance (ABS). The second major contributor to uncertainties in PP_UniMI measurements of MAAP spots was the fixed value of the asymmetry factor g=0.75: a sensitivity test on ABS (the quantity directly obtained from PP_UniMI measurements) calculated with lower g values, as often reported in the literature, showed that this can be up to 8% higher than the one obtained with g=0.75 as set in the MAAP. A smaller effect (<3%) on σ_{ap} retrieved on MAAP spots was due to the reconstruction of the angular distribution of scattered light using analytical functions instead of exploiting PP_UniMI high angular resolution. Furthermore, also the role of blank filter variability was investigated and the resulting contribution was less than 5%, which is comparable to MAAP instrumental unit-to-unit variability (Müller et al., 2011).
It is noteworthy that the present work took into account data from different sampling campaigns and sites; the described effects did not appear to depend significantly on the aerosol type.

In this study, only PP_UniMI data at 635 nm were employed to allow a direct comparison with MAAP (operating at 637 nm only). However, measurements at 5 wavelengths are routinely performed with the in-house made polar photometers set at the Universities of Milan (PP_UniMI) and Genoa (MWAA). Multi-λ analyses of MAAP spots could provide useful additional information about the spectral behaviour of σ_{ap} of the aerosol sampled by the MAAP. Indeed, these multi-wavelength data can be used in optical source- or component-apportionment models to estimate different contributions to σ_{ap} also measured in past campaigns, thus allowing e.g. a retrospective trend analysis. Moreover, they can serve as reference to evaluate and optimise correction schemes for on-line instruments measuring light transmission as a proxy for aerosol absorption.

Acknowledgements

The authors acknowledge the Italian Ministry of Research and the National Institute of Nuclear Physics for having supported this research in the PRIN2007-project and the INFN-TRACCIA experiment, respectively. The authors are also grateful to the GEMMA centre in the framework of project MIUR "Dipartimenti di Eccellenza 2018-2022". Measurements at Spanish sites (Montseny, Montsec and Barcelona) were supported by the Spanish Ministry of Economy, Industry and Competitiveness and FEDER funds under the project HOUSE (CGL2016-78594-R) and by the Generalitat de Catalunya (AGAUR 2014 SGR33, AGAUR 2017 SGR41 and the DGQA).

References

ACTRIS Intercomparison Workshop for Integrating Nephelometer and Absorption Photometers. (2013). https://www.wmo-gaw-wcc-aerosol-physics.org/files/actris-intercomparison-workshop-integrating-nephelometer-and-absorption-photometer-02-03-2013.pdf

Ammerlaan, B. A. J., Holzinger, R., Jedynska, A. D., & Henzing, J. S. (2017). Technical note: Aerosol light absorption measurements with a carbon analyser – Calibration and precision estimates. *Atmospheric Environment*, *164*, 1–7. https://doi.org/10.1016/j.atmosenv.2017.05.031

Andrews, E., Sheridan, P. J., Fiebig, M., McComiskey, A., Ogren, J. A., Arnott, P., Covert, D., Elleman, R., Gasparini, R., Collins, D., Jonsson, H., Schmid, B., & Wang, J. (2006). Comparison of methods for deriving aerosol asymmetry parameter. *Journal of Geophysical Research*, *111*(D5), D05S04. https://doi.org/10.1029/2004JD005734

Baumgardner, D., Popovicheva, O., Allan, J., Bernardoni, V., Cao, J., Cavalli, F., Cozic, J., Diapouli, E., Eleftheriadis, K., Genberg, P. J., Gonzalez, C., Gysel, M., John, A., Kirchstetter, T. W., Kuhlbusch, T. A. J., Laborde, M., Lack, D., Müller, T., Niessner, R., … Viana, M. (2012). Soot reference materials for instrument calibration and intercomparisons: a workshop summary with recommendations. *Atmospheric Measurement Techniques*, *5*(8), 1869–1887. https://doi.org/10.5194/amt-5-1869-2012

Bernardoni, V., Valli, G., & Vecchi, R. (2017). Set-up of a multi wavelength polar photometer for off-line absorption coefficient measurements on 1-h resolved aerosol samples. *Journal of Aerosol Science*, *107*, 84–93. https://doi.org/10.1016/j.jaerosci.2017.02.009

Bernardoni V., Ferrero L., Bolzacchini E., Forello A.C., Gregorič A., Massabò D., Močnik G., Prati P., Rigler M., Santagostini L., Soldan F., Valentini S., Valli G., Vecchi R.; Determination of Aethalometer multiple-scattering enhancement parameters and impact on source and component apportionment during the winter 2017-2018 EMEP/ACTRIS/COLOSSAL campaign in Milan; Atmospheric Measurement

Techniques Discussion. https://doi.org/10.5194/amt-2020-233

Bernardoni V., Ferrero L., Soldan F., Valentini S., Massabò D., Močnik G., Gregorič A., Cataldi M., Bolzacchini E., Prati P., Valli G., & Vecchi R. (2019, August). Multi-wavelength aerosol absorption coefficient measurements: instrument inter-comparison and implications for source and component apportionment; Poster session presentation at the European Aerosol Conference EAC2019, Gothenburg, Sweden.

Bond, T. C., Doherty, S. J., Fahey, D. W., Forster, P. M., Berntsen, T., DeAngelo, B. J., Flanner, M. G., Ghan, S., Kärcher, B., Koch, D., Kinne, S., Kondo, Y., Quinn, P. K., Sarofim, M. C., Schultz, M. G., Schulz, M., Venkataraman, C., Zhang, H., Zhang, S., … Zender, C. S. (2013). Bounding the role of black carbon in the climate system: A scientific assessment. *Journal of Geophysical Research: Atmospheres*, *118*(11), 5380–5552. https://doi.org/10.1002/jgrd.50171

Bond, Tami. C., Anderson, T. L., & Campbell, D. (1999). Calibration and Intercomparison of Filter-Based Measurements of Visible Light Absorption by Aerosols. *Aerosol Science and Technology*, *30*(6), 582–600. https://doi.org/10.1080/027868299304435

Chow, J. C., Watson, J. G., Doraiswamy, P., Chen, L.-W. A., Sodeman, D. A., Lowenthal, D. H., Park, K., Arnott, W. P., & Motallebi, N. (2009). Aerosol light absorption, black carbon, and elemental carbon at the Fresno Supersite, California. *Atmospheric Research*, *93*(4), 874–887. https://doi.org/10.1016/j.atmosres.2009.04.010

Collaud Coen, M., Weingartner, E., Apituley, A., Ceburnis, D., Fierz-Schmidhauser, R., Flentje, H., Henzing, J. S., Jennings, S. G., Moerman, M., Petzold, A., Schmid, O., & Baltensperger, U. (2010). Minimizing light absorption measurement artifacts of the Aethalometer: evaluation of five correction algorithms. *Atmospheric Measurement Techniques*, *3*(2), 457–474. https://doi.org/10.5194/amt-3-457-2010

D'Almeida G., Koepke P., & Shettle E.P. (1991). Atmospheric Aerosols: Global Climatology and Radiative Characteristics. A. Deepak Pub

Donateo, A., Lo Feudo, T., Marinoni, A., Dinoi, A., Avolio, E., Merico, E., Calidonna, C., Contini, D., & Bonasoni, P. (2018). Characterization of In Situ Aerosol Optical Properties at Three Observatories in the Central Mediterranean. *Atmosphere*, *9*(10), 369. https://doi.org/10.3390/atmos9100369

Drinovec, L., Močnik, G., Zotter, P., Prévôt, A. S. H., Ruckstuhl, C., Coz, E., Rupakheti, M., Sciare, J., Müller, T., Wiedensohler, A., & Hansen, A. D. A. (2015). The "dual-spot" Aethalometer: an improved measurement of aerosol black carbon with real-time loading compensation. *Atmospheric Measurement Techniques*, *8*(5), 1965–1979. https://doi.org/10.5194/amt-8-1965-2015

Ferrero, L., Močnik, G., Cogliati, S., Gregorič, A., Colombo, R., & Bolzacchini, E. (2018). Heating Rate of Light Absorbing Aerosols: Time-Resolved Measurements, the Role of Clouds, and Source Identification. *Environmental Science & Technology*, *52*(6), 3546–3555. https://doi.org/10.1021/acs.est.7b04320

Ferrero L., Cataldi M., Bigogno A., Bernardoni V., Soldan F., Valentini S., Massabò D., Močnik G., Gregorič A., Prati P., Valli G., Vecchi R. & Bolzacchini E. (2019, August). COLOSSAL winter campaign 2018: Experimental heating rate of light absorbing aerosol (black carbon, brown carbon) in Milan. Oral session presentation at the European Aerosol Conference EAC2019, Gothenburg, Sweden.

Formenti, P., Andreae, M. O., & Lelieveld, J. (2000). Measurements of aerosol optical depth above 3570 m asl in the North Atlantic free troposphere: Results from ACE-2. *Tellus, Series B: Chemical and Physical Meteorology*. https://doi.org/10.1034/j.1600-0889.2000.00006.x

Hänel, G. (1987). Radiation Budget of the Boundary Layer. Part II: Simultaneous Measurement of Mean Solar volume Absorption and Extinction Coefficients of Particles. *Beiträge Zur Physik Der Atmosphäre*, *60*(2).

Hänel, G. (1994). Optical properties of atmospheric particles: complete parameter sets obtained through polar photometry and an improved inversion technique. *Applied Optics*, *33*(30), 7187. https://doi.org/10.1364/AO.33.007187

Hansen, A. D. A., Rosen, H., & Novakov, T. (1984). The aethalometer — An instrument for the real-time measurement of optical absorption by aerosol particles. *Science of The Total Environment*, *36*, 191–196. https://doi.org/10.1016/0048-9697(84)90265-1

Hartley, W. S., & Hobbs, P. V. (2001). An aerosol model and aerosol-induced changes in the clear-sky albedo off the east coast of the United States. *Journal of Geophysical Research: Atmospheres*, *106*(D9), 9733–9748. https://doi.org/10.1029/2001JD900025

Horvath, H., Kasahara, M., Tohno, S., Olmo, F. J., Lyamani, H., Alados-Arboledas, L., Quirantes, A., & Cachorro, V. (2016). Relationship between fraction of backscattered light and asymmetry parameter. *Journal of Aerosol Science*, *91*, 43–53. https://doi.org/10.1016/j.jaerosci.2015.09.003

Horvath, Helmuth, Alados Arboledas, L., & Olmo Reyes, F. J. (2018). Angular scattering of the Sahara dust aerosol. *Atmospheric Chemistry and Physics*, *18*(23), 17735–17744. https://doi.org/10.5194/acp-18-17735-2018

Hyvärinen, A.-P., Vakkari, V., Laakso, L., Hooda, R. K., Sharma, V. P., Panwar, T. S., Beukes, J. P., van Zyl, P. G., Josipovic, M., Garland, R. M., Andreae, M. O., Pöschl, U., & Petzold, A. (2013). Correction for a measurement artifact of the Multi-Angle Absorption Photometer (MAAP) at high black carbon mass concentration levels. *Atmospheric Measurement Techniques*, *6*(1), 81–90. https://doi.org/10.5194/amt-6-81-2013

IPCC. (2013). Climate Change 2013 - The Physical Science Basis. In T. F. Stocker, D. Qin, G. K. Plattner, M. M. B. Tignor, S. K. Allen, J. Boschung, A. Nauels, Y. Xia, V. Bex, & P. M. Midgley (Eds.), *Climate Change 2013 the Physical Science Basis: Working Group I Contribution to the Fifth Assessment Report of the Intergovernmental Panel on Climate Change*. Cambridge University Press, Cambridge, United Kingdom and New York, NY, USA,. https://doi.org/10.1017/CBO9781107415324

Lack, D. A., & Cappa, C. D. (2010). Impact of brown and clear carbon on light absorption enhancement, single scatter albedo and absorption wavelength dependence of black carbon. *Atmospheric Chemistry and Physics*, *10*(9), 4207–4220. https://doi.org/10.5194/acp-10-4207-2010

Linnet, K. (1990). Estimation of the linear relationship between the measurements of two methods with proportional errors. *Statistics in Medicine*, *9*(12), 1463–1473. https://doi.org/10.1002/sim.4780091210

Massabò, D., Bernardoni, V., Bove, M. C., Brunengo, A., Cuccia, E., Piazzalunga, A., Prati, P., Valli, G., & Vecchi, R. (2013). A multi-wavelength optical set-up for the characterization of carbonaceous particulate matter. *Journal of Aerosol Science*, *60*, 34–46. https://doi.org/10.1016/j.jaerosci.2013.02.006

Massabò, D., Caponi, L., Bernardoni, V., Bove, M. C., Brotto, P., Calzolai, G., Cassola, F., Chiari, M., Fedi, M. E., Fermo, P., Giannoni, M., Lucarelli, F., Nava, S., Piazzalunga, A., Valli, G., Vecchi, R., & Prati, P. (2015). Multi-wavelength optical determination of black and brown carbon in atmospheric aerosols. *Atmospheric Environment*, *108*, 1–12. https://doi.org/10.1016/j.atmosenv.2015.02.058

Modini, R. L., Bukowiecki, N., Wehner, B., Müller, M., Tuch, T., Pfeifer, S., Henzing, J. S., Moerman, M. M., Fetfatzis, P., Gini, M., Eleftheriadis, K., Zanatta, M., Herber, A., Laj, P., Marinoni, A., Orsini, D., Cristofanelli, P., Gilardoni, S., & Gysel, M. (2018). *Deliverable D11.4: Report on closure results between the measurements of absorption coefficient and black carbon concentration*. https://www.actris.eu/Portals/46/Documentation/actris2/Deliverables/public/WP11_D11.4_M42.pdf?ver=2018-11-12-143124-623

Moosmüller, H., & Ogren, J. A. (2017). Parameterization of the Aerosol Upscatter Fraction as Function of the Backscatter Fraction and Their Relationships to the Asymmetry Parameter for Radiative Transfer

Calculations. *Atmosphere*, *8*(12), 133. https://doi.org/10.3390/atmos8080133

Müller, T., Henzing, J. S., de Leeuw, G., Wiedensohler, A., Alastuey, A., Angelov, H., Bizjak, M., Collaud Coen, M., Engström, J. E., Gruening, C., Hillamo, R., Hoffer, A., Imre, K., Ivanow, P., Jennings, G., Sun, J. Y., Kalivitis, N., Karlsson, H., Komppula, M., … Wang, Y. Q. (2011). Characterization and intercomparison of aerosol absorption photometers: result of two intercomparison workshops. *Atmospheric Measurement Techniques*, *4*(2), 245–268. https://doi.org/10.5194/amt-4-245-2011

Nordmann, S., Birmili, W., Weinhold, K., Wiedensohler, A., Mertes, S., Müller, K., Gnauk, T., Herrmann, H., Pitz, M., & Cyrys, J. (2009). Atmospheric aerosol measurements in the German Ultrafine Aerosol Network (GUAN). *Gefahrst. Reinhalt. L*, *69*(11), 137–145.

Ogren, J. A. (2010). Comment on "Calibration and Intercomparison of Filter-Based Measurements of Visible Light Absorption by Aerosols." *Aerosol Science and Technology*, *44*(8), 589–591. https://doi.org/10.1080/02786826.2010.482111

Pandolfi, M., Alados-Arboledas, L., Alastuey, A., Andrade, M., Angelov, C., Artiñano, B., Backman, J., Baltensperger, U., Bonasoni, P., Bukowiecki, N., Collaud Coen, M., Conil, S., Coz, E., Crenn, V., Dudoitis, V., Ealo, M., Eleftheriadis, K., Favez, O., Fetfatzis, P., … Laj, P. (2018). A European aerosol phenomenology – 6: scattering properties of atmospheric aerosol particles from 28 ACTRIS sites. *Atmospheric Chemistry and Physics*, *18*(11), 7877–7911. https://doi.org/10.5194/acp-18-7877-2018

Park, K., Chow, J. C., Watson, J. G., Trimble, D. L., Doraiswamy, P., Park, K., Arnott, W. P., Stroud, K. R., Bowers, K., Bode, R., Petzold, A., & Hansen, A. D. A. (2006). Comparison of Continuous and Filter-Based Carbon Measurements at the Fresno Supersite. *Journal of the Air & Waste Management Association*, *56*(4), 474–491. https://doi.org/10.1080/10473289.2006.10464521

Petzold, A., Kramer, H., & Schönlinner, M. (2002). Continuous Measurement of Atmospheric Black Carbon Using a Multi-angle Absorption Photometer. *Environmental Science & Pollution Research*.

Petzold, A., Ogren, J. A., Fiebig, M., Laj, P., Li, S.-M., Baltensperger, U., Holzer-Popp, T., Kinne, S., Pappalardo, G., Sugimoto, N., Wehrli, C., Wiedensohler, A., & Zhang, X.-Y. (2013). Recommendations for reporting "black carbon" measurements. *Atmospheric Chemistry and Physics*, *13*(16), 8365–8379. https://doi.org/10.5194/acp-13-8365-2013

Petzold, A., Schloesser, H., Sheridan, P. J., Arnott, W. P., Ogren, J. A., & Virkkula, A. (2005). Evaluation of Multiangle Absorption Photometry for Measuring Aerosol Light Absorption. *Aerosol Science and Technology*, *39*(1), 40–51. https://doi.org/10.1080/027868290901945

Petzold, Andreas, & Schönlinner, M. (2004). Multi-angle absorption photometry—a new method for the measurement of aerosol light absorption and atmospheric black carbon. *Journal of Aerosol Science*, *35*(4), 421–441. https://doi.org/10.1016/j.jaerosci.2003.09.005

R Core Team. (2020). *R: A language and environment for statistical computing*. R Foundation for Statistical Computing, Vienna, Austria. https://www.r-project.org/

Rama Gopal, K., Arafath, S. M., Lingaswamy, A. P., Balakrishnaiah, G., Pavan Kumari, S., Uma Devi, K., Siva Kumar Reddy, N., Raja Obul Reddy, K., Penchal Reddy, M., Reddy, R. R., & Suresh Babu, S. (2014). In-situ measurements of atmospheric aerosols by using Integrating Nephelometer over a semi-arid station, southern India. *Atmospheric Environment*, *86*, 228–240. https://doi.org/10.1016/j.atmosenv.2013.12.009

Ripley, B. D., & Thompson, M. (1987). Regression techniques for the detection of analytical bias. *The Analyst*, *112*(4), 377. https://doi.org/10.1039/an9871200377

Samset, B. H., Stjern, C. W., Andrews, E., Kahn, R. A., Myhre, G., Schulz, M., & Schuster, G. L. (2018). Aerosol Absorption: Progress Towards Global and Regional Constraints. *Current Climate Change Reports*, *4*(2), 65–83. https://doi.org/10.1007/s40641-018-0091-4

Sandradewi, J., Prévôt, A. S. H., Szidat, S., Perron, N., Alfarra, M. R., Lanz, V. A., Weingartner, E., & Baltensperger, U. (2008). Using Aerosol Light Absorption Measurements for the Quantitative Determination of Wood Burning and Traffic Emission Contributions to Particulate Matter. *Environmental Science & Technology*, *42*(9), 3316–3323. https://doi.org/10.1021/es702253m

Saturno, J., Pöhlker, C., Massabò, D., Brito, J., Carbone, S., Cheng, Y., Chi, X., Ditas, F., Hrabě de Angelis, I., Morán-Zuloaga, D., Pöhlker, M. L., Rizzo, L. V., Walter, D., Wang, Q., Artaxo, P., Prati, P., & Andreae, M. O. (2017). Comparison of different Aethalometer correction schemes and a reference multi-wavelength absorption technique for ambient aerosol data. *Atmospheric Measurement Techniques*, *10*(8), 2837–2850. https://doi.org/10.5194/amt-10-2837-2017

Sheridan, P. J., Arnott, W. P., Ogren, J. A., Andrews, E., Atkinson, D. B., Covert, D. S., Moosmüller, H., Petzold, A., Schmid, B., Strawa, A. W., Varma, R., & Virkkula, A. (2005). The Reno Aerosol Optics Study: An Evaluation of Aerosol Absorption Measurement Methods. *Aerosol Science and Technology*, *39*(1), 1–16. https://doi.org/10.1080/027868290901891

Slowik, J. G., Cross, E. S., Han, J.-H., Davidovits, P., Onasch, T. B., Jayne, J. T., Williams, L. R., Canagaratna, M. R., Worsnop, D. R., Chakrabarty, R. K., Moosmüller, H., Arnott, W. P., Schwarz, J. P., Gao, R.-S., Fahey, D. W., Kok, G. L., & Petzold, A. (2007). An Inter-Comparison of Instruments Measuring Black Carbon Content of Soot Particles. *Aerosol Science and Technology*, *41*(3), 295–314. https://doi.org/10.1080/02786820701197078

Vecchi, R., Bernardoni, V., Paganelli, C., & Valli, G. (2014). A filter-based light-absorption measurement with polar photometer: Effects of sampling artefacts from organic carbon. *Journal of Aerosol Science*, *70*, 15–25. https://doi.org/10.1016/j.jaerosci.2013.12.012

Virkkula, A., Ahlquist, N. C., Covert, D. S., Arnott, W. P., Sheridan, P. J., Quinn, P. K., & Coffman, D. J. (2005). Modification, Calibration and a Field Test of an Instrument for Measuring Light Absorption by Particles. *Aerosol Science and Technology*, *39*(1), 68–83. https://doi.org/10.1080/027868290901963

Weber P., Bundke U., Bischof O., Fischer B., Berg M., & Petzold A. (2019, August). Multi-spectral aerosol optical properties of different types of light absorbing and light scattering aerosols obtained from closure studies. Oral presentation at the European Aerosol Conference EAC2019, Gothenburg, Sweden.

Weingartner, E., Saathoff, H., Schnaiter, M., Streit, N., Bitnar, B., & Baltensperger, U. (2003). Absorption of light by soot particles: determination of the absorption coefficient by means of aethalometers. *Journal of Aerosol Science*, *34*(10), 1445–1463. https://doi.org/10.1016/S0021-8502(03)00359-8